Crystal Chemistry and Magnetic Properties of Gd-substituted Aurivillius-type $Bi_5FeTi_3O_{15}$ Ceramics

Vladimir Koval[1]†, Ivan Skorvanek[2], Giuseppe Viola[3], Man Zhang[3], Chenglong Jia[4] and Haixue Yan[3]

1 *Institute of Materials Research, Slovak Academy of Sciences, Watsonova 47, 04001 Kosice, Slovakia*
2 *Institute of Experimental Physics, Slovak Academy of Sciences, Watsonova 47, 04001 Kosice, Slovakia*
3 *School of Engineering and Materials Science, Queen Mary, University of London, Mile End Road, London E1 4NS, United Kingdom*
4 *Key Laboratory for Magnetism and Magnetic Materials of the Ministry of Education, Lanzhou University, Tianshui Road No. 222, Lanzhou 730000, People's Republic of China*

† Corresponding author, e-mail: vkoval@saske.sk

Abstract

Aurivillius-phase ferroelectrics can be turned into multiferroic materials by incorporating magnetic ions. The four-layer Aurivillius-type system $Bi_5FeTi_3O_{15}$ is well known to show a strong magnetoelectric effect; however, much controversy exists on its magnetic state and the possible multiferroicity at room temperature.

In this paper, we report a detailed investigation on the interconnections between crystal chemistry and magnetic properties of $Bi_5FeTi_3O_{15}$ ceramics chemically modified by the A-site gadolinium substitution. The structural studies showed that all $Bi_{5-x}Gd_xFeTi_3O_{15}$ ($0 \leq x \leq 1$) samples adopt the polar orthorhombic space group symmetry $A2_1am$ at room temperature. The unit cell volume and the orthorhombic distortion decrease alongside the reduction of octahedral tilts by increasing the amount of Gd added. The decrease in tilting distortion of the $[Ti/Fe]O_6$ octahedra was further evidenced by the suppression of the Raman $A_1[111]$ tilt mode at 233 cm^{-1}. By using superconducting quantum interference and vibrating sample magnetometry, it was demonstrated that all the ceramics are paramagnetic from 5 K up to 700 K. It was thus concluded that the A-site substitution of $Bi_5FeTi_3O_{15}$ with magnetic Gd ions brings about a slight structural relaxation of the parental orthorhombic lattice, but it is not an effective way to induce multiferroic properties in the Aurivillius compound. We suggest that the room-temperature (ferri/ferro/antiferro-) magnetism in $Bi_5FeTi_3O_{15}$ previously reported in the literature might be due to the presence of magnetic impurities or local short-range magnetic ordering formed during material processing under different conditions.

I. Introduction

Nowadays, magnetoelectric multiferroics derived from ferroelectric Aurivillius-phase $Bi_4Ti_3O_{12}$ (BIT) are receiving considerable attention from materials scientists and device designers for the development of new generation memories and spintronic devices.[1,2] BIT is well known for its excellent ferroelectric properties (large spontaneous polarization and high fatigue resistance) existing up to a very high temperature.[3] The crystal structure of BIT is characterized by three perovskite-like unit cells sandwiched between fluorite-type structured $(Bi_2O_2)^{2+}$ layers along the *c*-axis. It represents an archetype of the Aurivillius-type structure[4] of general formula $Bi_2A_{n-1}B_nO_{3n+3}$ ($[Bi_2O_2]^{2+}[A_{n-1}B_nO_{3n+1}]^{2-}$, with three perovskite-like layers (n = 3) per unit cell, in which the cube-octahedral site A is occupied by the 12-coordinated Bi^{3+} cation and the octahedral site B is filled by the 6-coordinated Ti^{4+} cation. The large spontaneous polarization appearing in such structure when BIT is cooled through the Curie temperature is due to displacements of Bi cations along the [100] direction and the corresponding cooperative tilting and distortion of TiO_6 octahedra occurring to relieve the lattice stress induced by the structural transition from a paraelectric, nonpolar tetragonal phase (space group *I*4/*mmm*) to a ferroelectric orthorhombic *B*2*cb* phase.[5]

By incorporating magnetic cations in their lattice, the bismuth layered Aurivillius phase compounds were found to exhibit multiferroic properties.[6] Besides the natural ferroelectricity, a magnetic order was reported to exist in BIT when Ti^{4+} ions are partially substituted, for instance, by Fe^{3+} ions at the B-sites.[7] The A-sites of BIT can accommodate rare earth cations, making it possible to suppress leakage currents[8] and consequently improve the ferroelectric properties by reducing the amount of oxygen vacancies.[9] Contradictory evidence on the substitution effect in the A-site of BIT has been reported by Oh *et al.*[10], who found that the introduction of lanthanum ions into the lattice suppresses the spontaneous polarization.

Recently, a number of theoretical and experimental studies on bismuth-based Aurivillius materials with various compositions and different number of perovskite-type layers, including materials based on four-layer compounds such as $Bi_5FeTi_3O_{15}$ (BFTO), have been conducted to develop a single-phase multiferroic with large magnetoelectric coupling at room temperature.[11,12] Although their thermal stability decreases with increasing n number[13], it has been shown that 4- to 6-layer compositions are single-phase materials, which exhibit multiferroic properties at room temperature. High values of the room-temperature magnetoelectric coefficient have been reported for BFTO[14]; however, paramagnetic behavior with no magnetic long-range order down to 2 K was observed in polycrystalline films[14] and bulk ceramics[15]. Earlier studies on BFTO suggested a weakly ferromagnetic state at room

temperature[16] or a *G*-type collinear antiferromagnetic structure occurring below the Neél temperature $T_N \sim 80$ K[17]. Additional contradictory and scattered data were found on the crystal structure and ferroelectric Curie temperature of BFTO, both strongly dependent on the synthesis method and annealing conditions.[18-20] For the room-temperature phase of BFTO single crystals, the orthorhombic space group *Fmm*2 has been suggested by Kubel and Schmid in 1991 based on X-ray diffraction data.[19] Later, Hervoches *et al.*[21], using powder neutron diffraction, revealed that the crystal structure of this 4-layer Aurivillius phase at room temperature adopts a lower symmetry space group $A2_1am$, which, unlike the *Fmm*2 symmetry, allows not only atomic displacements along the polar *a* axis, but also the tilting of the oxygen octahedra. For the ferroelectric-paraelectric phase transition, various values of the ferroelectric Curie temperature T_c between 885 and 1075 K were reported in the literature[13,19,20], depending on the processing and characterization methods.

A partial substitution of bismuth by lanthanides has been found to improve the ferroelectric properties and enhance the magnetoelectric coupling in Aurivillius multiferroics.[22,23] Peña *et al.*[24] have showed that rare-earth (including Gd) substituted BFTO ceramics are isostructural with pure BFTO and exhibit a paramagnetic behavior at and below room temperature. On the other hand, Huang *et al.*[25] reported a weakly ferromagnetic state in Nd-modified BFTO at room temperature. Very recently, the A-site substitution with Gd^{3+} ions was found to significantly enhance the room-temperature ferromagnetism in $Bi_{4.25}Gd_{0.75}Fe_{0.5}Co_{0.5}Ti_3O_{15}$ ceramics.[26] It was demonstrated that the remanent magnetization of the $Bi_{4.25}Gd_{0.75}Fe_{0.5}Co_{0.5}Ti_3O_{15}$ sample is about four times higher (18.5 memu/g) than that of $Bi_5Fe_{0.5}Co_{0.5}Ti_3O_{15}$ (~ 4 memu/g).

In order to clarify the above-mentioned discrepancies about the structure evolution and formation of magnetic long-range order in 4-layer Aurivillius-phase BFTO compounds upon introducing magnetically-active rare earth ions with 4*f* electrons, we performed a systematic investigation of the substitutional effect of Gd^{3+} ions on the crystal structure chemistry and magnetic properties of $Bi_{5-x}Gd_xFeTi_3O_{15}$ ceramics ($x = 0 – 1$). It is well known that the trivalent gadolinium ion has strongly localized *f*-electrons and carries a large magnetic moment, if compared with the diamagnetic Bi^{3+} ion. In addition, the radius of Gd^{3+} is smaller than that of Bi^{3+},[26] which may affect the structural distortion in the Aurivillius materials. Hence, both the ionic mismatch-driven variations in structural parameters, including bond lengths and bond angles, as well as the magnetic contribution of the rare earth ions are considered in this study to potentially establish or enhance the long-range magnetic ordering in BFTO. X-ray diffraction (XRD), Raman scattering, Superconducting Quantum Interference Device (SQUID) and

Vibrating Sample Magnetometry (VSM) techniques are used to study the crystal structure and magnetic properties of the ceramics synthesized by the solid-state reaction method. The Rietveld analysis of the room-temperature XRD data allowed determining the changes in lattice parameters and atomic coordinates due to substitution. The magnetic behavior of pure and Gd-substituted BFTO (Gd-BFTO) ceramics is characterized in a wide temperature interval 5 - 600 K via the temperature dependence of the zero-field-cooling (ZFC) and field-cooling (FC) magnetization and of the magnetic hysteresis loops.

II. Experimental Section

Polycrystalline samples of the $Bi_{5-x}Gd_xFeTi_3O_{15}$ series (x = 0, 0.15, 0.30, 0.50, 0.7 and 1) were prepared by a conventional two-stage solid-state reaction method using the oxides Bi_2O_3, Gd_2O_3, Fe_2O_3 and TiO_2 (all with high purity ≥ 99.995, Sigma-Aldrich). The calcination of the mixed powders was carried in air at 1073 K (for x = 0 and 0.15), 1093 K (for x = 0.30 and 0.50) and 1113 K (for x = 1) for 5 h with heating/cooling rates of 10 K/min. The calcined powders were uniaxially pressed at 150 MPa into pellets of 12 mm diameter and a thickness of about 1 mm. The disks were sintered in sealed alumina crucibles at 1313 K (for x = 0 and 0.15) and 1233 K (for $0.30 \leq x \leq 1$ and La doped) for 5 h in a programmable laboratory furnace. The density of the sintered samples, as determined by the Archimedes method, was about 90 - 92% of the theoretical density.

The crystal structure of the samples was studied by X-ray diffraction using an automated Philips X'Pert Pro diffractometer with Cu K_α radiation. The XRD data collected over the angular range of $20^0 \leq 2\theta \leq 130^0$ were analysed by a full profile matching method using the FullProf software package[27]. In addition, a hard X-ray micro-diffraction experiment was performed at the beamline I15 at the Diamond Light Source (Didcot, Oxfordshire, UK; electron storage ring operating at an energy of 3 GeV with beam current ~ 300 mA operating in top-up mode) in order to unambiguously determine the space group of the ceramics. During the experiment, a monochromatic synchrotron radiation of photon energy 76.01 keV (λ = 0.01631 nm) was used. The beam of photons was first focused by compound refractive lenses down to the size of 100 μm and then collimated on the sample to a spot size of 20 μm diameter. The samples were illuminated by highly intense hard X-rays for 8 seconds. The resulting 2D XRD patterns were recorded using a Perkin Elmer 1621 detector. The recorded XRD patterns were then processed using the Fit2D software[28] and analysed by the Rietveld refinement method[27].

A micro-probe XploRa system (Horiba/Jobin-Yvon, France) in back-scattering geometry was used for acquisition of the room-temperature Raman scattering spectra from an unpolished surface of the pellets. The 532 nm line of an argon ion laser, focused through a 100x (numerical aperture of 0.9) microscope objective lens, served as an excitation source. The laser power distributed on the pellet surface over a spot with diameter smaller than 1 μm (in the focal plane) was held below 3 mW in order to avoid any sample heating. The data were collected by a Peltier-cooled charged coupled device camera in the spectral range from 20 cm^{-1} to 1000 cm^{-1} with a step of 1.858 cm^{-1} and an integration time of 10 s. The micro-Raman scattering spectra were fitted and the spectral peaks positions (the Raman shifts in cm^{-1}) identified using a Horiba Scientific's LabSpec 5 suite software. X-ray absorption fine-structure (XAFS) measurements were performed at the beamline P65 located at the PETRA III synchrotron storage ring. Spectroscopic data in the range of 6960 - 7912 eV were collected in fluorescence mode using a fixed-exit double-crystal Si(111) monochromator. During all XAFS measurements, the samples were irradiated by an X-ray beam with a cross-section of 2 x 0.4 mm (width x height). The X-ray intensities were monitored using ionization chambers filled by nitrogen (18% absorption). The fluorescence detector (Passivated Implanted Planar Silicon PIPS) was placed approximately 10 cm away from the sample and at an angle of 45^0 with respect to the incoming X-ray beam.

The cryogenic magnetic properties of the samples were investigated using a SQUID magnetometer (MPMS XL-5, Quantum Design). The magnetic field dependent magnetization was recorded at 300 K and 5 K in an external magnetic field of ± 5 T. The magnetic data at elevated temperatures were acquired using a MicroSense EV9 VSM unit. The temperature dependence of the magnetization was measured in two temperature intervals: 5 K - 300 K (SQUID) and 300 K – 750 K (VSM), under zero-field cooling (ZFC) and field-cooling (FC) conditions.

III. Results and Discussion

X-ray diffraction

The stacked plot in Fig. 1a compares the room-temperature XRD patterns of Gd-BFTO ceramics with various amount of gadolinium added. At first sight, one can notice that the angular positions of the diffraction lines of pure BFTO do not change substantially upon substitution and for all compositions the obtained Bragg reflections closely match with those reported in the literature[21] which are based on the orthorhombic distorted structure of

$Bi_5FeTi_3O_{15}$ (JCPDS Card No. 01-089-8545). The results of the search-and-match analysis (Fig. 1b) on synchrotron XRD data showed that the crystallographic *figures-of-merit* (*FoM*, the quality of the agreement of experimental and reference pattern peak positions) for the orthorhombic $A2_1am$ phase reaches a slightly higher value (*FOM* = 0.723) for all the samples investigated than that of the BFTO phase with the *Fmm*2 space group symmetry (*FOM* = 0.692, JCPDS Card No. 01-082-0063), as initially described by Kubel and Schmid.[19]

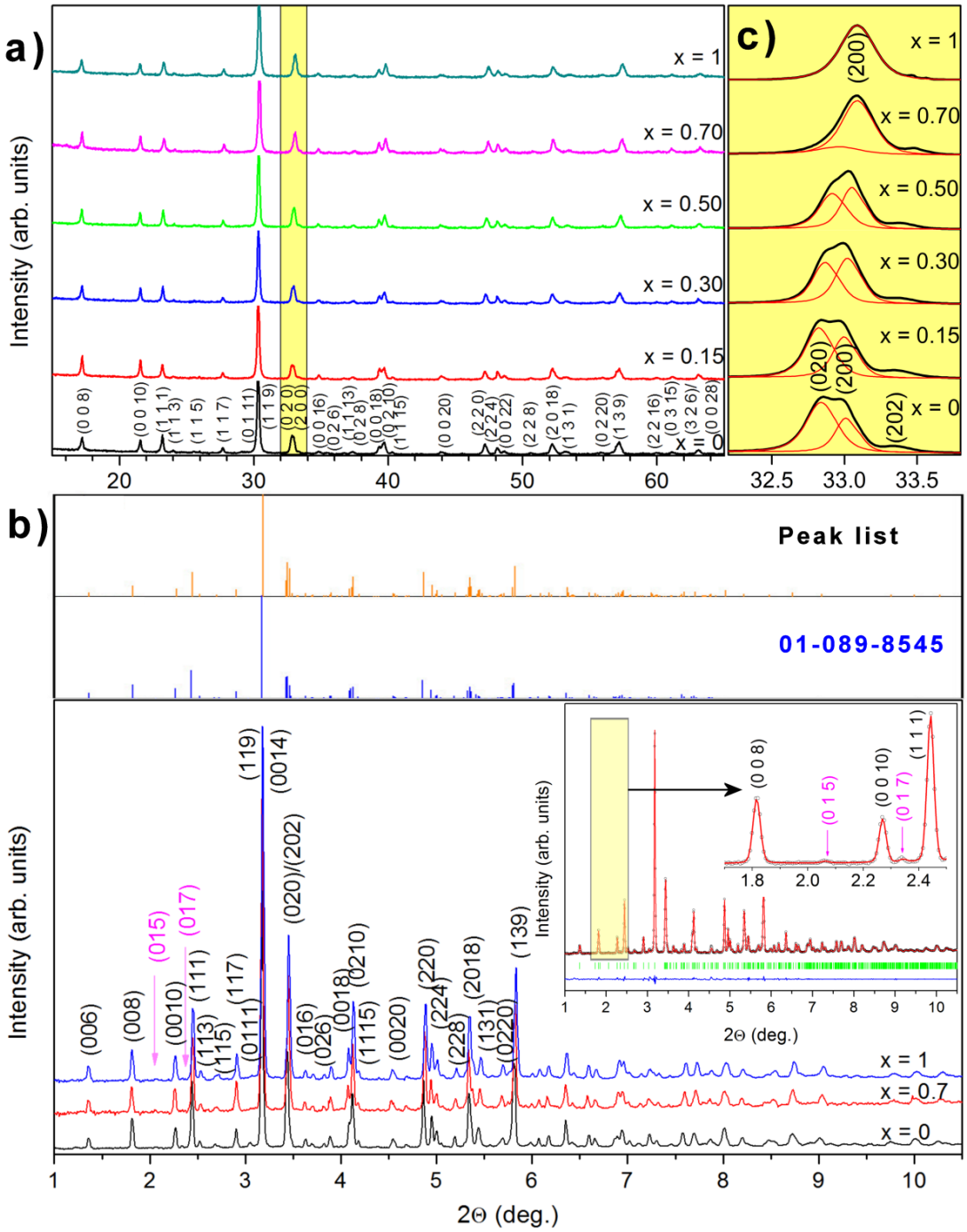

Figure 1. (a) XRD patterns collected from $Bi_{5-x}Gd_xFeTi_3O_{15}$ ($0 \leq x \leq 1$) ceramics at room temperature. (b) Synchrotron X-ray diffractograms of the representative samples (x = 0, 0.7 and

1). The upper inset illustrates the phase matching of the x = 0 sample and the reference BFTO (JCPDS Card No. 01-089-8545) with space group $A2_1am$. The right inset shows the results of the Rietveld refinement of the room-temperature XRD data of BFTO, including the evidence of the $A2_1am$ peaks (015) and (017). (c) Enlarged views of the XRD patterns around 33^0 to show the evolution of the orthorhombic doublet (020) (200) on doping.

Furthermore, the structure refinements with the $A2_1am$ structural model (the inset of Fig. 1b) allowed assigning the weak peaks at $2\theta = 2.063^0$ and 2.344^0 to the (015) and (017) planes reflections, respectively, at a photon energy of 76.01 keV. By using neutron powder diffraction, Hevroches *et al.*[21] demonstrated that the room-temperature ferroelectric phase of the Aurivillius-phase $Bi_5FeTi_3O_{15}$ is indeed $A2_1am$. This structure has been predicted to possess the maximum degree of ideal symmetry allowed in a ferroelectric Aurivillius phase with an even number of perovskite-like layers.[29] No additional peaks corresponding to possible impurity phases[30] are observed in the diffractograms within the detection limit of the instrument, indicating the formation of Aurivillius single phase. The full width at half maximum (FWHM) of the most intense peak (119) is about ~ 0.3^0, which implies a good crystallinity of the ceramics. Fig. 1c shows the enlarged area around $2\theta \approx 33^0$ with two closely overlapping orthorhombic (020) and (200) peaks. The Fourier deconvolution of the double peak revealed that upon doping the relative 2θ difference between the peaks decreases with a slight shift towards higher angles. The right-shift in 2θ position indicates a reduction in *d*–spacing, suggesting a decrease in the unit cell volume.

To further explore the substitution-induced structural changes in the Aurivillius phase, we performed full pattern matching for each composition at room temperature. The diffraction intensity *vs*. Bragg angle dependences were modelled in the orthorhombic space group $A2_1am$ by a pseudo-Voight function (Supplementary Material, Fig. S1). The calculated lattice parameters with the corresponding values of the goodness of fit (GOF), χ^2, are listed in Table S1 in the Supplementary Material. Fig. 2 displays the variation of the lattice parameters as a function of the Gd content added. From the figure, one can see that the cell parameters *a* (~ 5.459 Å for x = 0) and *b* (~ 5.433 Å) decrease almost linearly following the Vegard's law[31] and become closer to each other upon substitution, whereas along the *c* direction the structure expands with increasing Gd content. As a consequence, both the unit cell volume (*V*) and orthorhombic distortion ($\delta = 2(a - b)/(a + b)$) are progressively reduced upon doping (see Table S1 and the inset of Fig. 3). These observations are in accordance with the structural studies

recently reported for other rare-earth substituted Aurivillius compounds.[9,23,32] Paul *et al.*[9] observed similar substitution-induced relaxation of the structural distortion in the $Bi_{4-x}Sm_xTi_{3-x}Fe_xO_{12\pm\delta}$ system and attributed it to different ionic radii of the substituting (Sm^{3+}, Fe^{3+}) and substituted (Bi^{3+}, Ti^{4+}) ions. Moreover, they found that the 3-layer orthorhombically-distorted system transforms to a higher symmetry tetragonal phase at a critical concentration (x = 0.4) of the substituting elements. In our 4-layer Aurivillius material, no such structural phase transition is observed at room temperature within the concentration range investigated ($0 \leq x \leq 1$). The incorporation of Gd^{3+} ions into BFTO introduces only a slight shrinkage of the Aurivillius phase unit cell. It is thought that the extended concentration range of phase stability of the orthorhombic phase in Gd-BFTO, if compared to that of the 3-layer Aurivillius compounds, can be related to the increased number of perovskite-like slabs and to a higher orthorhombic distortion ($\delta \sim 4.87\text{x}10^{-3}$ *vs.* $2.02\text{x}10^{-3}$ in *Ref.* 9 for x = 0 compositions).

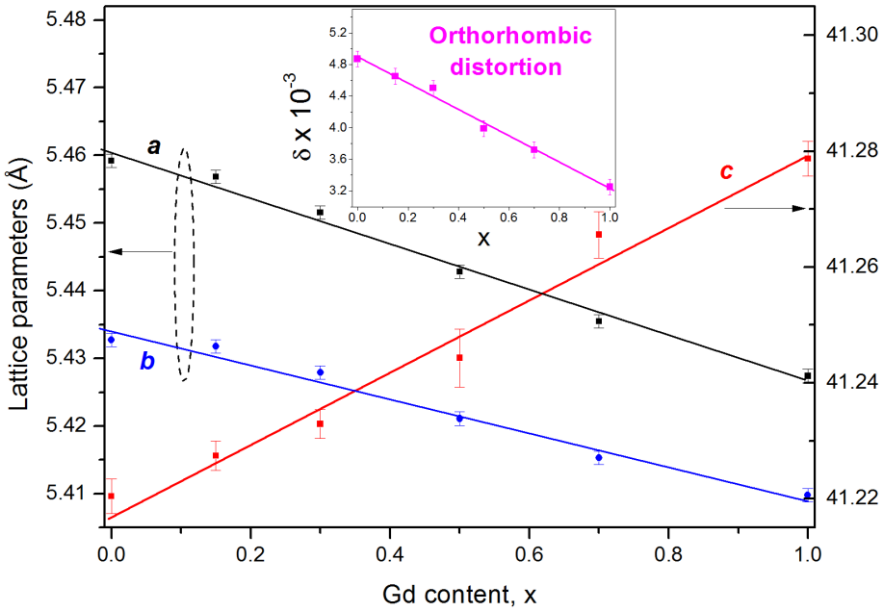

Figure 2. Gd-substitution induced structural change in $Bi_{5-x}Gd_xFeTi_3O_{15}$ ceramics.

Considering a possible change in the octahedral tilt system, which often accompanies lattice deformation in the rare-earth modified perovskites with the tolerance factor t < 1[33], oxygen octahedral rotations across the perovskite-like slabs in the 4-layer Aurivillius material were also investigated. In order to obtain more accurate information on the local environment of the B sites in BFTO and its variations upon the A-site Gd substitution, the diffraction data obtained for the x = 0 and x = 1 samples by a monochromatic synchrotron radiation were analyzed using the Rietveld method. The initial structural data were taken from previous studies

by Hervoches *et al.*[21]. As the position of the origin of the polar axis is not defined in the $A2_1am$ space group, it was fixed by assuming that the x coordinate of the Bi(1) atom is equal to 0.25. The Ti and Fe cations were set to occupy the same position in the center of each BO_6 unit in the perovskite-like layers with a fixed occupancy ratio Ti/Fe = 3/1 (3/4 for Ti and 1/4 for Fe). The isotropic atomic displacement parameters (ADPs) were constrained to be equivalent. According to the structural refinements of Aurivillius structures with a lower number of layers ($n \leq 3$)[5,35], rare earth cations tend to preferentially occupy a more symmetrical environment, i.e. the A-sites of the perovskite-like blocks. However, Chu *et al.*[32] have recently indicated that a partial cation mixing or the so called cation disorder may exist at the A-sites of the perovskite-like slabs and fluorite-like layers. In order to examine the cation disorder in the 4-layer $Bi_{5-x}Gd_xFeTi_3O_{15}$ system, we introduced a non-zero occupancy of Gd(3) atoms (the 8-fold A-site of fluorite-type units) in our Rietveld refinements. The results showed that the Gd^{3+} ions exclusively enter the 12-fold A-site of perovskite-type, and the Bi^{3+}/Gd^{3+} disorder, if exists in these structures, is negligible. While the resultant occupancy of gadolinium atoms in the perovskite-like layers was found to be 0.316, the refined occupancy for Gd(3) was about 0.0039, which is less than 1.5% of the sum of Gd(1) and Gd(2) occupancies. The smaller Gd atoms are randomly distributed over the A-sites of the inner and outer perovskite-type layers with the corresponding occupancies of Gd(1) and Gd(2), the sum of which is about a quarter of the Bi(1) + Bi(2) occupancy (2/3 in outer slabs and 1/3 in inner perovskite blocks), validating the stoichiometric ratio of Bi:Gd = 4:1 in $Bi_4GdFeTi_3O_{15}$. The ADPs and the atomic positions of the A-site cations in the perovskite-like layers and those of Bi^{3+}/Gd^{3+} in the fluorite-like layer were considered as equivalent. The isotropic thermal factors of oxygens were fixed at reasonable values (taken from *Ref.* 21) and not further refined in order to stabilize the refinement. The Rietveld analysis revealed that the octahedral tilt along the *c*-axis in the inner and outer perovskite-like layers of the crystal structure decreases upon Gd substitution. Table S2 (in the Supplementary Material) summarizes the refined fractional coordinates of the atoms, the selected bond distances and the angles in the structure of the selected compounds. Obviously, due to the inherent insensitivity of X-ray diffraction to oxygen positions in materials containing heavy atoms such as Bi or Gd, the values of the estimated standard deviations (ESDs, in parentheses) for atomic coordinates of O(1) – O(8) are much larger than that of Bi^{3+}/Gd^{3+} ions. From the table, one can see that both the O(3)-O(1)-O(3) and O(1)-O(3)-O(5) non-bonded contact angles, which represent a measure of the tilting around the *a* and *b* axes, respectively, are lower for $Bi_5FeTi_3O_{15}$ than those for $Bi_4GdFeTi_3O_{15}$ (the inset of Fig. 3 illustrates the evolution of the O(3)-O(1)-O(3) contact angle). Analogously, the bond angles of the Ti/Fe - O

- Fe/Ti chains along the *c*-axis in the inner and outer octahedral layers of the crystal structure increase from 155.35(5)^0 to 157.42(49)^0 and from 154.27(9)^0 to 161.70(22)^0, respectively, when x is increased from 0 to 1.

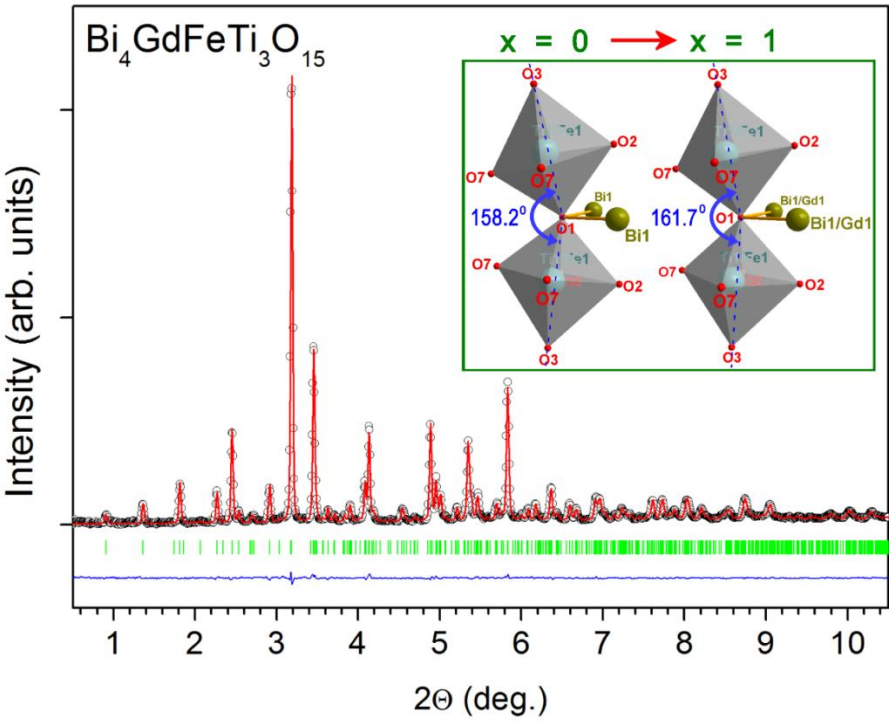

Figure. 3 Rietveld plot for the refinement of $Bi_4GdFeTi_3O_{15}$ ceramics in space group $A2_1am$. The inset illustrates the substitution-driven suppression of the tilting distortion of oxygen octahedra in the inner layers.

As demonstrated in Table S2 and presented graphically in Fig. 3, in the 4-layer $Bi_{5-x}Gd_xFeTi_3O_{15}$ system, the structural changes associated with the substitution-induced suppression of the orthorhombic distortion (structural relaxation) are dominated by the reducing octahedral tilt. Other geometrical distortions of the Aurivillius structure associated, for instance, with alternations inside the perovskite octahedron or the relative displacements of cations in the fluorite-like layer against the apical oxygen in the outer perovskite layer[32], are minor. In Fig. 4, it is evident that upon the Gd substitution both the Bi(3)-Bi(3) bond lengths and the O(6)-O(6) distances in the fluorite-like layer remain unchanged within the range of the experimental error (see schematics in the figure below). Hence, the interlayer strain due to size mismatch between perovskite-like slabs and fluorite-like units does not change with x, which is reflected in a stable structural configuration of the adjacent $[Ti(2)/Fe(2)]O_6$ octahedra, in particular, in the *ab* plane (see Table S2). In addition, almost the same distances of bismuth atoms and oxygens in the

fluorite-like layer relative to apical oxygen O(5) in the outer perovskite-like layer were found in the end member compositions (x = 0 and x = 1), which again rules out the possibility of any substantial A-site cation mixing[32] in the fluorite-like layer and its effect on the composition-driven structural relaxation. On the other hand, the increase of Bi(1)-O(1) bond lengths in the *ab* plane suggests that the addition of Gd^{3+} ions significantly affects the local environment of B-site cations in the inner perovskite-like slabs. This behaviour is supportive of the inherent mechanism of the substitution-induced increasing lattice symmetry, resulting in the suppression of the orthorhombic distortion via the reduced octahedral tilting in the 4-layer Gd-substituted BFTO Aurivillius compounds.

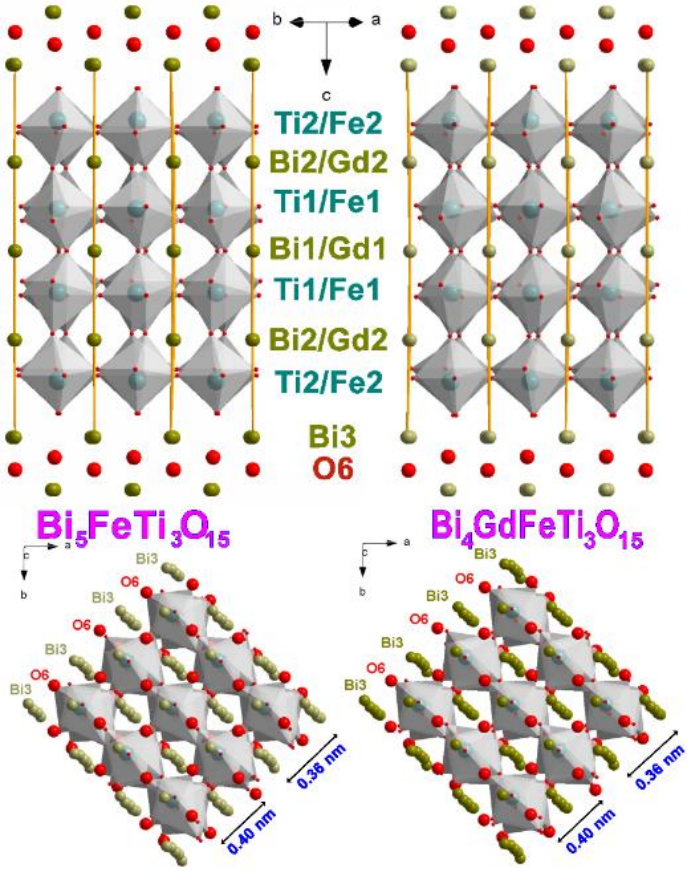

Figure. 4 Crystal structure models of $Bi_5FeTi_3O_{15}$ (left) and $Bi_4GdFeTi_3O_{15}$ (right) in view of (010) direction (above) and along *c*-axis (below).

Since the *hkl*, *khl* reflection pairs such as *020*, *200* nearly merge to each other for the x = 1 composition (see Fig. 1c), the room-temperature XRD data of this sample were further tested for a possible coexistence of the orthorhombic $A2_1am$ phase and the tetragonal phase with *I*4/*mmm* space group (Fig. 2b). The *I*4/*mmm* (space group # 139) symmetry has been

suggested for the high temperature phase of $Bi_4FeTi_3O_{15}$ (> 1020 K) and the room-temperature phase of structurally-related $Na_{0.5}Bi_{4.5}Ti_4O_{15}$ compounds.[34] However, it has been also observed at room temperature in Gd- and La-substituted $Bi_4Ti_3O_{12}$ ceramics.[32,35] The numerical fitting of the XRD pattern of the $Bi_4GdFeTi_3O_{15}$ sample by the Rietveld method under the assumption of a mixed ($A2_1am$ + $I4/mmm$) structural model showed that the Bragg reflections of both phases are overlapping, thus making it difficult to distinguish the orthorhombic peaks (200)/(020) and tetragonal peak (110) from each other. The two-phase model, however, revealed a dominant contribution of the orthorhombic phase (> 90%) over the non-polar tetragonal structure, if such higher symmetry phase really exists in the x = 1 sample. In order to ascertain the existence of the tetragonal phase in Gd-BFTO ceramics, we analysed the changes of the FWHM with the variations of the Gd concentration for the most intensive reflection *119* and for the reflection pair *200, 020*. It was found that the FWHM of the *119* peak (the most intense peak, I/I_0 = 100 %, where I and I_0 are the intensities of the reflection peak and background, respectively) and the reflection pair (I/I_0 = 30 %) do not change significantly upon doping (~ 0.3^0 in 2θ), which precludes the existence of the phase transition within the concentration range studied.

Raman scattering

Further details of the structural evolution of Gd-BFTO ceramics were investigated more explicitly through the analysis of the Raman spectra. Raman spectroscopy has been demonstrated to be a very useful technique to study phase transitional characteristics and local structure modulation in $BiFeO_3$-derived and Aurivillius-phase multiferroic materials.[9,33,36] In comparison with XRD, where the structural information is averaged over about 10^4 unit cells (a long-range probe), Raman scattering explores short-range structural order, and thus offers better sensitivities for probing local structural distortions, such as octahedral tilting and ionic displacements that are coherent over a short length scale of about few unit cells.

The room-temperature Raman spectra of $Bi_{5-x}Gd_xFeTi_3O_{15}$ (x = 0 – 1) ceramics are shown in Fig. 5. From the figure, it is clear that the spectral profiles of all the studied compositions are very similar to each other and resemble the characteristic vibrational modes of the orthorhombic $A2_1am$ phase of pure $Bi_5FeTi_3O_{15}$.[37] This observation is in accordance with the XRD results and evidences that the parental orthorhombic structure does not vary significantly with Gd substitution. According to earlier theoretical studies based on factor-group analysis[37], the phonon modes in the vibrational spectra of pure $Bi_5FeTi_3O_{15}$ below 200 cm^{-1} can be ascribed to the A-site cations (Bi^{3+}), while those above 200 cm^{-1} with A_{1g} character result from the torsion, bending and stretching of oxygen octahedra. The most intense low

frequency peak at about 58 cm^{-1} reflects the vibrations of Bi^{3+} ions in $(Bi_2O_2)^{2-}$ layers. By fitting the measured spectra with a Gaussian-Lorentzian mixed function and decomposing the fitted Raman lines into individual components using the LabSpec program, it was found that the position of this mode does not change upon Gd substitution. Thus, it appears that the insertion of a perovskite $Bi_{1-x}Gd_xFeO_3$ block into BIT does not affect the fluorite-like Bi_2O_2 layers.

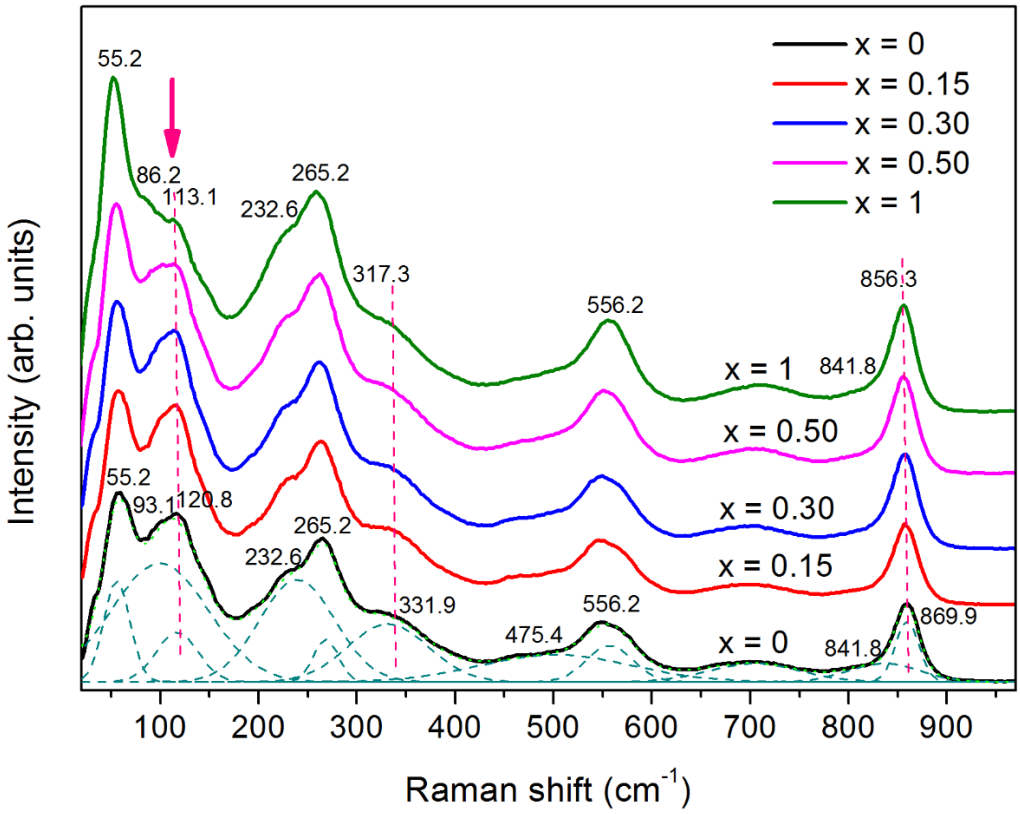

Figure 5. Raman spectra collected from $Bi_{5-x}Gd_xFeTi_3O_{15}$ ceramics at room temperature. The dashed dark cyan lines, displayed below the measured spectra, are the spectral peaks corresponding to the Raman active modes of BFTO, as obtained by fitting the respective Raman line (x = 0).

The soft Raman modes between 80 and 170 cm^{-1} are closely associated with the vibrations of the Bi^{3+} and Gd^{3+} ions at the A-site positions of the perovskite-like slabs. From the vibrational point of view, they can be considered as external modes because of the collective motion of A-site cations against the slightly distorted oxygen octahedra. In this low frequency region, a significant change in the phonon characteristics, suggesting a reduced degree of A – O covalent bonding in highly doped samples, is observed. The triplet spectral peak originating from the Raman active modes of BFTO at around 93 cm^{-1}, 121 cm^{-1} and 151 cm^{-1} progressively decreases in intensity and shifts to lower frequencies with increasing Gd amount. At x = 1, the

most prominent peak at 121 cm^{-1} nearly disappears, indicating the onset of a composition-driven transition to a non-polar phase. Considering that the A-site vibrations in $BiFeO_3$-related compounds are predominantly caused by the stereochemical activity of the $6s^2$ lone pair electrons in Bi^{3+}, which are responsible for the appearance of the spontaneous ferroelectric polarization (ferroelectricity) in these multiferroics[38], the observed suppression of the spectral triplet peak upon Gd substitution is thought to be brought by the reduced degree of Bi – O hybridization in perovskite-type slabs of the Aurivillius phase due to the dilution of Bi lone pairs by Gd doping, as Gd^{3+} does not have an ns^2 lone pair. Thus, the A-site substitution with the Gd^{3+} ions may result in the suppression of the ferroelectric long-range ordering in BFTO ceramics.

The double peak centered around 250 cm^{-1} is related to the overlapping of B_{2g} and B_{3g} orthorhombic phonon modes, which can be ascribed to the O – Ti/Fe – O bending vibrations. The Raman mode at 233 cm^{-1} should be inactive in case of perfect octahedral O_h arrangement of the BO_6 octahedron. However, due to the distortion of the octahedra, the phonon mode at 233 cm^{-1}, the so-called A_1[111] tilt mode, is often observed in perovskite oxides.[33,37] The suppression of this mode and the increase in the spectral intensities ratio of the B_{2g} and B_{3g} modes (not shown here) with increasing gadolinium can be attributed to the decreasing tilting distortion of the [Ti/Fe]O_6 octahedra, and hence the decrease of the orthorhombic distortion δ, as demonstrated by XRD (see Table S1 and Table S2 in the Supplementary Material).

Similarly, due to the substitution-induced change in the strength of Bi – O bonds followed by the relaxation of the orthorhombic distortion, the stretching modes of the oxygen octahedra observed as a double peak at 546 cm^{-1} and 559 cm^{-1} in pure $Bi_5FeTi_3O_{15}$ (x = 0) tend to merge with each other upon Gd substitution. Mao *et al.*[36] assigned the lower frequency mode (left side of the double peak) to TiO_6 octahedra and that on the right side to the stretching vibrations of the FeO_6 octahedra in BFTO. The progressive overlapping of these Raman phonon modes gives rise to the increased spectral intensity of the peak observed at 556 cm^{-1} for the x = 1 composition.

The weak modes at around 330 and 480 cm^{-1} have been assigned to the oscillations related to the ferroelectricity and the opposing extensions of the external apical oxygen atoms of the BO_6 octahedra, respectively.[39] The ferroelectric peak at 330 cm^{-1}, analogous to that at 121 cm^{-1}, decreases in intensity and shifts towards lower vibrational frequency as the amount of Gd increases. Converse trends in compositional behavior of the torsional and stretching modes from BO_6 octahedra are observed in the Raman spectra near 700 cm^{-1} and 857 cm^{-1}, respectively. While the former (torsion of the octahedra in the *a*-*b* plane) shifts towards higher

vibrational frequency, the Raman frequency of the stretching mode (stretching of the octahedra along *c*-axis) decreases as the amount of gadolinium increases. This indicates that the A-site substitution with Gd^{3+} ions alters the local structural environment around the $[Ti/Fe]O_6$ octahedra in the perovskite-type slabs in an anisotropic manner. Thus, the observed evolution of the Raman modes well correlates with the structural changes identified by X-ray diffraction, where the addition of Gd was found to decrease the contact angle O(8)-O(4)-O(8) in the outer octahedra, while those representing the tilting around the *a*/*b* axes (i.e., O(3)-O(1)-O(3) and O(1)-O(3)-O(5)) increased with increasing x (see Table S2 in the Supplementary Material).

Magnetic properties

The magnetization *vs*. magnetic field (M-H) curves of $Bi_{5-x}Gd_xFeTi_3O_{15}$ ceramics (x = 0, 0.15, 0.3, 0.5 and 1) measured at 300 K and 5 K are shown in Fig. 6a. At room temperature, the field dependence of the magnetization in all the investigated compositions demonstrates a linear character, typical of paramagnets. No noticeable hysteresis or remanent magnetization was observed even at very low temperatures (the inset of Fig. 6a), which indicates that the A-site Gd substitution does not affect the magnetic state of the parent $Bi_5FeTi_3O_{15}$ phase. By measuring the temperature dependence of the magnetization under field cooling (FC), and zero field cooling (ZFC) conditions at a magnetic field of 200 Oe, the paramagnetic behavior of the samples was confirmed to exist down to 5 K (Fig. 6b). Both the FC and ZFC magnetizations continuously increase with decreasing temperature and show a reversible thermo-magnetic behavior in the temperature range considered.

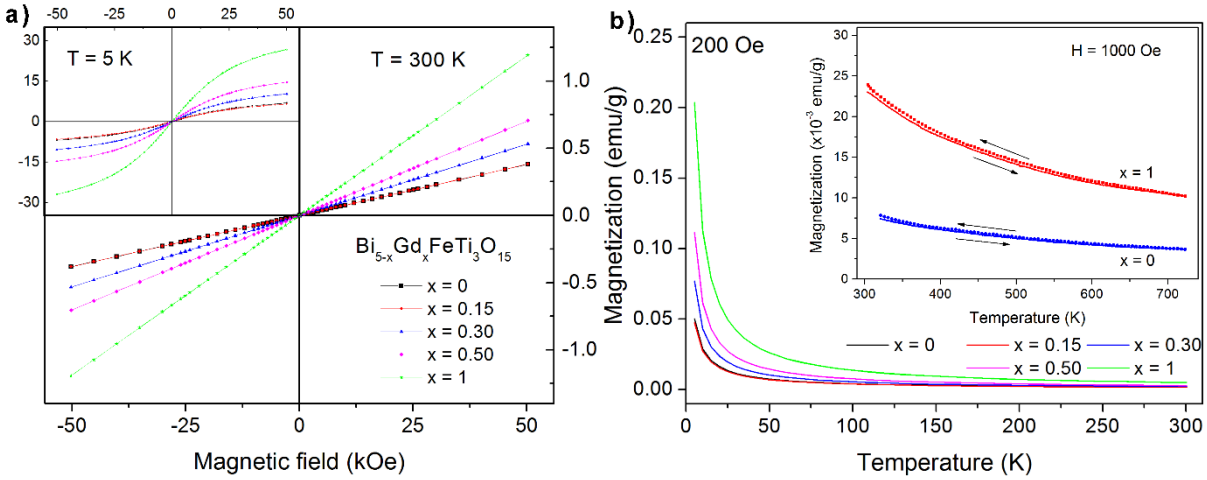

Figure 6. (a) Field dependences of the magnetization obtained for $Bi_{5-x}Gd_xFeTi_3O_{15}$ ceramics at T = 300 K and T = 5 K (inset). (b) Temperature dependences of the magnetization for $Bi_{5-x}Gd_xFeTi_3O_{15}$ samples at H = 200 Oe. The inset demonstrates paramagnetic behavior of the

$Bi_5FeTi_3O_{15}$ and $Bi_4GdFeTi_3O_{15}$ samples in the temperature range of 300 – 750 K (H = 1000 Oe).

In contrast to previous magnetic studies which suggested a magnetic transition in pure BFTO and rare-earth substituted BFTO compounds[9,14,17,23,26], no magnetic anomaly related to a possible transition at cryogenic temperatures is observed in the magnetization vs temperature plots (Fig. 6b). Moreover, the high-temperature VSM magnetometry showed that the paramagnetic behavior of all the samples in the $Bi_{5-x}Gd_xFeTi_3O_{15}$ series exists up to 700 K. Therefore, we suggest that the room-temperature (ferri/ferro/antiferro-) magnetism in BFTO previously reported in the literature might be due to the presence of magnetic impurities or short-range ordered spins in randomly distributed Fe-rich nanoregions formed during material processing under different conditions. As shown in the inset of Fig. 6b, the magnetization of both the end composition samples (x = 0 and x = 1) subjected to an external magnetic field of 1000 Oe slowly decreases with increasing temperature from room temperature to 700 K, and, reversely, it increases on cooling obeying the modified Curie-Weiss law[40]:

$$\chi = C/(T - T_{CW}) + \chi_0 \quad (1)$$

, where χ is the magnetic susceptibility ($\chi = M/H$), T is the temperature and T_{CW} is the critical Curie-Weiss temperature. The constants C and χ_0 represent the material-related Curie constant and the temperature-independent magnetic contributions, respectively. By fitting the temperature-dependent magnetization data for the x = 0 and x = 1 samples (Fig. 7, red line), the Curie-Weiss temperature, which reflects the strength of the interaction between magnetic moments, is obtained. The calculated values of T_{CW} are -4.95(3) K and -2.80(2) K for $Bi_5FeTi_3O_{15}$ and $Bi_4GdFeTi_3O_{15}$, respectively, which imply the existence of a very weak antiferromagnetic coupling in both the end-member compositions at low temperatures. Table S3 (in the Supplementary Material) summarizes the values of the modified Curie-Weiss law parameters (χ_0, C and paramagnetic T_{CW}) obtained for the x = 0, 0.3, 0.5 and 1 samples by fitting of the temperature dependence of the reciprocal mass susceptibility ($1/\chi_\sigma$) in the temperature range from 50 K up to 200 K. Below 50 K and above 200 K a distinct deflection from the modified Curie-Weiss law is observed, as shown in Fig. 7.

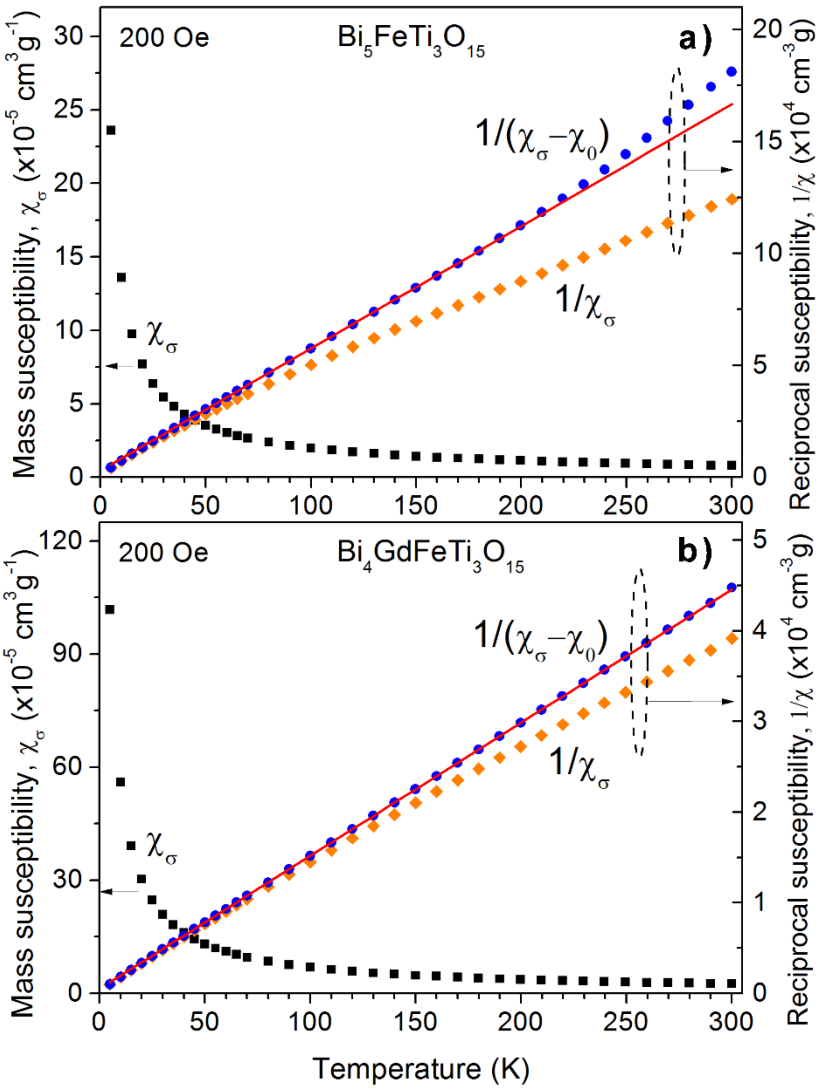

Figure 7. Temperature dependence of the magnetic mass susceptibility and Curie-Weiss law fitting of the reciprocal susceptibility for (a) $Bi_5FeTi_3O_{15}$ and (b) $Bi_4GdFeTi_3O_{15}$ subjected to a magnetic field of 200 Oe.

The effective magnetic moment derived from the corresponding Curie constant *C* using the formula:[40]

$$\mu_{eff} = \sqrt{\frac{3k_B CM}{N_A \mu_B^2}} \approx \sqrt{8CM} \qquad (2)$$

, where k_B is the Boltzmann constant, *M* is the molar mass of the respective compound, N_A is the Avogadro number and μ_B is the Bohr magneton, was found to increase upon Gd substitution from μ_{eff} = 3.75(1)μ_B for pure BFTO to μ_{eff} = 8.76(1)μ_B for $Bi_4GdFeTi_3O_{15}$. The experimental value of the effective magnetic moment for BFTO is consistent with previous studies for $BiFeO_3$-derived compounds[33] and iron-substituted Aurivillius phase materials[41] and reflects the presence of the intermediate-spin Fe^{3+} ions in the Aurivillius structure. The 3+ oxidation state of iron and gadolinium in the Aurivillius structure was confirmed by the Near-Edge X-ray

Absorption Fine Structure (NEXAFS) spectroscopy. Fig. S2 (in the Supplementary Material) shows the Fe-K edge XAFS spectra of the representative x = 0.7 sample and the reference powders of magnetite (Fe_3O_4, mixed Fe^{2+}/Fe^{3+} valence state of iron[42]) and hematite (α-Fe_2O_3, valence state Fe^{3+}, in *Ref.* 42). From the figure, the spectral similarity of the Gd-substituted BFTO sample and hematite in shape and position of the absorption edge is obvious. Similarly, the position of Gd-L_3 edge at about 7245 eV (inset in Fig. S2) is in agreement with that reported for Gd-based oxides with the trivalent gadolinium ions[43].

Under assumption that the spin quantum number S can be formalized as[40]:

$$S = {}^1/_2\left(\sqrt{1+\left({}^{2\mu_{eff}}/_{g}\right)^2}-1\right) \quad (3)$$

, where g is the gyromagnetic factor (g = 2), the obtained μ_{eff} = 3.75(1)μ_B for BFTO corresponds to spin S = 1.4405(1). The ground electronic state of Gd^{3+} is $^8S_{7/2}$ with seven unpaired electrons (theoretical angular moment J = 7/2) and the calculated effective magnetic moment is μ_{eff} = 7.94μ_B. Taking into account the contributions of both the Gd^{3+} ions and intermediate-spin Fe^{3+} ions to the net magnetization, the total paramagnetic effective moment of the Gd-substituted BFTO samples can be determined within a mean field approximation[40] from the expression $\mu_{eff}^2 = \upsilon g^2 S(S+1)\mu_B^2$, where υ is the fraction of magnetic ions per formula unit. For instance, the expected effective magnetic moment of $Bi_4GdFeTi_3O_{15}$ μ_{eff} = 8.78(1)μ_B is close to that obtained from the Curie-Weiss fit (see Table S3, μ_{eff} = 8.76(1)μ_B) implying that Fe^{3+} ions remain in the intermediate-spin state upon substitution and both the Fe^{3+} and Gd^{3+} ions contribute to the total magnetic moment. It is worth mentioning that the substitution-induced increase of the effective magnetic moment in the $Bi_{1-x}Gd_xFeTi_3O_{15}$ ceramic series (see Table S3 in the Supplementary Material) due to the progressive replacement of diamagnetic Bi^{3+} ions with the Gd^{3+} ions carrying a large magnetic moment is responsible for the observed enhancement of the paramagnetic magnetization at cryogenic and room temperatures, as shown in Fig. 6.

Apparently, the A-site substitution of perovskite-like units with large, magnetically-active Gd ions is not sufficient to establish multiferroicity not only in the 3-layer BIT Aurivillius phase as reported by Khomchenko *et al.*[35], but also in the 4-layer BFTO structure. In that respect, our findings are not supportive of the predictions reported in earlier theoretical and experimental studies[11,35], which have foreseen the rare-earth substitution combined with a partial replacement of Ti ions by a transition-metal Fe^{3+} ion at B-sites as an effective way to

introduce robust magnetic ordering in the ferroelectric BIT, and thus obtain a multiferroic material with a strong magnetoelectric coupling at room temperature. Mössbauer spectroscopy studies on single-phase bismuth-layer Aurivillius-type compounds (BFTO, and $n \geq 5$)[15,44] are in accordance with our observations, evidencing that these materials are paramagnets in a wide temperature range including room temperature (the paramagnetic behavior of these materials exists in a wide temperature range 2 - 350 K), regardless of the number of perovskite-like layers. Because of the low concentration of Fe^{3+} ions and their random occupancy of the octahedral B-sites[15,21], the probability of long-range ordering of the iron spins in BFTO is small, which makes the ferromagnetic exchange interaction practically impossible to be achieved at room temperature. The structural relaxation induced by the A-site Gd substitution is not capable of substantially changing the local environment of B-site cations and evenly distribute the Fe ions over the B-sites in the BFTO perovskite-like layers. Zhao *et al.*[14] have suggested that in BFTO there are Fe-rich nanoregions with Fe^{3+} cations magnetically short-range ordered, which are responsible for large magnetoelectric coupling at room temperature due to the antisymmetric Dzyaloshinskii-Moriya exchange interaction, analogous to that causing a weakly ferromagnetic state in the rare-earth substituted $BiFeO_3$[45]. Ferromagnetism has been found to be induced in BFTO by a partial replacement of the Fe^{3+} ions at the B-sites with other transition-metal ions such as Co^{3+} and Mn^{3+}.[6,36,46,47,48] However, the intrinsic multiferroicity in the co-doped Aurivillius materials is still under debate due to the possible formation of magnetically-active secondary phases.[30,49] According to our very recent study[50], Fe/Co co-substitution can induce intrinsic multiferroic properties in the three-layer $Bi_{3.25}La_{0.75}Ti_3O_{12}$ Aurivillius-type ceramics at and above room temperature. Based on these findings and aiming at introducing a magnetic long-range order in the four-layer BFTO-derived Aurivillius compounds, we have lately upgraded our Gd-BFTO system by the B-site Co co-substitution; its electronic and crystal structure alongside with the multiferroic properties are currently being investigated.

IV. Conclusions

The present study shows that upon Gd substitution the parent $A2_1am$ structure of $Bi_5FeTi_3O_{15}$ is preserved, while the unit cell volume and the orthorhombic distortion progressively decrease. Additionally, it was revealed that $Bi_5FeTi_3O_{15}$ is paramagnetic from cryogenic and until room temperature. The substitution of Bi^{3+} ions by Gd^{3+} ions at A-sites of the perovskite-like slabs is not capable of inducing any magnetic ordering in the 4-layer Aurivillius-type $Bi_{5-x}Gd_xFeTi_3O_{15}$

($0 \leq x \leq 1$) ceramics. It is proposed that multiferroic properties at room temperature can be achieved by co-substitution with aliovalent transition-metal ions in the B-sites.

Figures Captions

Figure 1. (a) XRD patterns collected from $Bi_{5-x}Gd_xFeTi_3O_{15}$ ($0 \leq x \leq 1$) ceramics at room temperature. (b) Synchrotron X-ray diffractograms of the representative samples (x = 0, 0.7 and 1). The upper inset illustrates phase matching of the x = 0 sample and the reference BFTO (JCPDS Card No. 01-089-8545) of a space symmetry group $A2_1am$. The right inset shows the results of the Rietveld refinement of the room-temperature XRD data of BFTO, including the evidence of the $A2_1am$ peaks (015) and (017). (c) Enlarged views of the XRD patterns around 33^0 to show the evolution of the orthorhombic doublet (020) (200) on doping.

Figure 2. Gd-substitution induced structural change in $Bi_{5-x}Gd_xFeTi_3O_{15}$ ceramics.

Figure. 3 Rietveld plot for the refinement of $Bi_4GdFeTi_3O_{15}$ ceramics in space group $A2_1am$. The inset illustrates the substitution-driven suppression of the tilting distortion of oxygen octahedra.

Figure. 4 Crystal structure models of $Bi_5FeTi_3O_{15}$ (left) and $Bi_4GdFeTi_3O_{15}$ (right) in view of (010) direction (above) and along c-axis (below).

Figure 5. Raman spectra collected from $Bi_{5-x}Gd_xFeTi_3O_{15}$ ceramics at room temperature. The dashed dark cyan lines, displayed below the measured spectra, are the spectral peaks corresponding to the Raman active modes of BFTO, as obtained by fitting the respective Raman line (x = 0).

Figure 6. (a) Field dependences of the magnetization obtained for $Bi_{5-x}Gd_xFeTi_3O_{15}$ ceramics at T = 300 K and T = 5 K (inset). (b) Temperature dependences of the magnetization for $Bi_{5-x}Gd_xFeTi_3O_{15}$ samples at H = 200 Oe. The inset demonstrates paramagnetic behavior of the $Bi_5FeTi_3O_{15}$ and $Bi_4GdFeTi_3O_{15}$ samples in the temperature range of 300 – 700 K (H = 1000 Oe).

Figure 7. Temperature dependence of the magnetic mass susceptibility and Curie-Weiss law fitting of the reciprocal susceptibility for (a) $Bi_5FeTi_3O_{15}$ and (b) $Bi_4GdFeTi_3O_{15}$ subjected to a magnetic field of 200 Oe.

Author Contributions

The manuscript was written through contributions of all authors. All authors have given approval to the final version of the manuscript.

Notes

The authors declare no competing financial interest.

Supporting Information

Figure S1. XRD plots for the profile refinement of (a) $Bi_5FeTi_3O_{15}$ and (b) $Bi_4GdFeTi_3O_{15}$ ceramics in space group $A2_1am$.

Figure S2. Fe-K edge and Gd-L_3 NEXAFS spectra of $Bi_{4.3}Gd_{0.7}FeTi_3O_{15}$ ceramics.

Table S1. Lattice parameters and orthorhombic distortion for $Bi_{5-x}Gd_xFeTi_3O_{15}$ ceramics at room temperature.

Table S2. Refined structural parameters and selected bond distances and bond angles for end-member compositions (x = 0 and 1) in the $Bi_{1-x}Gd_xFeTi_3O_{15}$ ceramic series obtained by Rietveld refinement of the room-temperature synchrotron XRD data (space group: $A2_1am$).

Table S3. Curie-Weiss parameters for $Bi_{5-x}Gd_xFeTi_3O_{15}$ ceramics obtained by fitting of the temperature dependence of the reciprocal magnetic susceptibility.

Acknowledgement

This work was partially supported by the Grant Agency of the Slovak Academy of Sciences under Grant No. 2/0059/17 and by the Slovak Research and Development Agency through grants APVV-15-0115 and SK-CN-2017-0004. V.K. acknowledges the help of K. Saksl (IMR

SAS, Kosice) and E. Mudra (IMR SAS, Kosice) in the X-ray synchrotron diffraction and Raman scattering measurements.

References

1 Bibes, M.; Barthelemy, A. Multiferroics: Towards a magnetoelectric memory, *Nat. Mater.* **2008**, *7*, 425-426.

2 Fusil, S.; Garcia, V.; Barthélémy, A.; Bibes, M. Magnetoelectric Devices for Spintronics, *Annu. Rev. Mater. Res.* **2014**, *44*, 91-116.

3 Subbarao, E.C. A family of ferroelectric bismuth compounds, *J. Phys. Chem. Solids* **1962**, *23*, 665-676.

4 Aurivillius, B. Mixed bismuth oxides with layer lattices, *Ark. Kemi.* **1949**, *1*, 463-471.

5 Newnham, R.E.; Wolfe, R.W.; Dorrian, J.F. Structural basis of ferroelectricity in the bismuth titanate family, *Mater. Res. Bull.* **1971**, *6*, 1029-1040.

6 Keeney, L.; Downing, C.; Schmidt, M.; Pemble, M.E.; Nicolosi, V.; Whatmore, R.W. Direct atomic scale determination of magnetic ion partition in a room temperature multiferroic material, *Sci. Rep.* **2017**, *7*, 1737.

7 Chen, X.Q.; Yang, F.J.; Cao, W.Q.; Wang, H.; Yang, C.P.; Wang, D.Y.; Chen, K. Enhanced multiferroic characteristics in Fe-doped Bi4Ti3O12 ceramics, *Solid State Commun.* **2010**, *150*, 1221-1224.

8 Long, Ch.; Fan, H.; Ren P. Structure, Phase Transition Behaviors and Electrical Properties of Nd Substituted Aurivillius Polycrystallines Na0.5NdxBi2.5–xNb2O9 (x = 0.1, 0.2, 0.3, and 0.5), *Inorg. Chem.* **2013**, *52*, 5045-5054.

9 Paul, J.; Bhardwaj, S.; Sharma, K.K.; Kotnala, R.K.; Kumar R. Room temperature multiferroic behaviour and magnetoelectric coupling in Sm/Fe modified Bi4Ti3O12 ceramics synthesized by solid state reaction method, *J. Alloys Compd.* **2015**, *634*, 58-64.

10 Oh, S.-J.; Shin, Y.; Tran, T.T.; Lee, D.W.; Yoon, A.; Halasyamani, P.S.; Ok, K.M. Structure–Property Relationships in Solid Solutions of Noncentrosymmetric Aurivillius Phases, Bi4–xLaxTi3O12 (x = 0–0.75), *Inorg. Chem.* **2012**, *51*, 10402-10407.

11 Birenbaum, A.Y.; Ederer, C. Potentially multiferroic Aurivillius phase Bi5FeTi3O15: Cation site preference, electric polarization, and magnetic coupling from first principles, *Phys. Rev. B* **2014**, *90*, 214109.

12 Rao, C.N.R.; Sundaresan, A.; Saha, R. Multiferroic and Magnetoelectric Oxides: The Emerging Scenario, *J. Phys. Chem. Lett.* **2012**, *3*, 2237-2246.

13 Lomanova, N.A.; Morozov, M.I.; Ugolkov, V.L.; Gusarov, V.V. Properties of Aurivillius phases in the Bi4Ti3O12-BiFeO3 system, *Inorg. Mater.* **2006**, *42*, 189-195.

14 Zhao, H.; Kimura, H.; Cheng, Z.; Osada, M.; Wang, J.; Wang, X.; Dou, S.; Liu, Y.; Yu, J.; Matsumoto, T. et al. Large magnetoelectric coupling in magnetically short-range ordered $Bi_5Ti_3FeO_{15}$ film, *Sci. Rep.* **2014**, *4*, 5255.

15 Jartych, E.; Pikula, T.; Kowal, K.; Dzik, J.; Guzdek, P.; Czekaj, D. Magnetoelectric Effect in Ceramics Based on Bismuth Ferrite, *Nanoscale Res. Lett.* **2016**, *11*, 234.
16 Mao, X.Y.; Wang, W.; Chen, X.B. Electrical and magnetic properties of Bi5FeTi3O15 compound prepared by inserting BiFeO3 into Bi4Ti3O12, *Solid State Commun.* **2008**, *147*, 186-189.
17 Srinivas, A.; Suryanarayana, S.V.; Kumar, G.S.; Kumar, M.M. Magnetoelectric measurements on Bi5FeTi3O15 and Bi6Fe2Ti3O18, *J. Phys: Condens. Matter.* **1999**, *11*, 3335-3340.
18 Mao, X.Y.; Wang, W.; Sun, H.; Lu, Y.; Chen, X. Influence of different synthesizing steps on the multiferroic properties of Bi5Fe1Ti3O15 and Bi5Fe0.5Co0.5Ti3O15 ceramics, *J. Mater. Sci.* **2012**, *47*, 2960-2965.
19 Kubel, F.; Schmid, H. X-ray room temperature structure from single crystal data, powder diffraction measurements and optical studies of the Aurivillius phase Bi5(Ti3Fe)O15, *Ferroelectrics* **1992**, *129*, 101-112.
20 Ismailadze, I.G. Crystal chemistry of perovskite-like layer type ferroelectrics, *J. Phys.* **1972**, Colloq. *2*, 237-239.
21 Hervoches, Ch.H.; Snedden, A.; Riggs, R.; Kilcoyne, S.H.; Manuel, P.; Lightfoot, P. Structural behavior of the four-layer Aurivillius-phase ferroelectrics SrBi4Ti4O15 and Bi5Ti3FeO15, *J. Solid State Chem.* **2002**, *164*, 280-291.
22 Prasad, N.V.; Kumar, G.S. Magnetic and magnetoelectric measurements on rare-earth-substituted five-layered Bi6Fe2Ti3O18 compound, *J. Magn. Magn. Mater.* **2000**, *213*, 349-356.
23 Ti, R.; Huang, F.; Zhu, W.; He, J.; Xu, T.; Yue, Ch.; Zhao, J.; Lu, X.; Zhu, J. Multiferroic and dielectric properties of Bi4LaTi3FeO15 ceramics, *Ceram. Int.* **2015**, *41*, S453-S457.
24 Peña, O.; Guizouarn, T.; Moure, C.; Gil, V.; Tartaj, J. Magnetic properties of Aurivillius lanthanide-bismuth (LnFeO3)nBi4Ti3O12 (n. = 1,2) layered titanates, *Bol. Soc. Esp. Ceram. V.* **2008**, *47*, 129-132.
25 Huang, F.; Lu, X.; Chen, C.; Lin, W.; Chen, X.; Zhang, J.; Liu, Y.; Zhu, J. Room-temperature multiferroic properties of Bi4.15Nd0.85Ti3FeO15 thin films prepared by the metal–organic decomposition method, *Solid State Commun.* **2010**, *150*, 1646-1649.
26 Zuo, X.Z.; Zhang, M.L.; He, E.J.; Yang, J.; Zhu, X.B.; Dai, J.M. Multiferroic property, dielectric response, and scaling behavior in Aurivillius Bi4.25Gd0.75Fe0.5Co0.5Ti3O15 ceramic, *J. Alloys Compd.* **2017**, *695*, 2556-2662.
27 http://www.ill.eu
28 Hammersley, A.P.; Svensson, S.O.; Hanfland, M.; Fitch, A.N.; Häusermann, D. Two-Dimensional Detector Software: From Real Detector to Idealised Image or Two-Theta Scan, *High Pressure Res.* **1996**, *14*, 235-248.
29 Rae, A.D.; Thompson, J.G.; Withers, R.L.; Wililis, A.C. Structure refinement of commensurately modulated bismuth titanate, Bi4Ti3012, *Acta Cryst. B* **1990**, *46*, 474-487.
30 Morozov, M.I.; Gusarov, V.V. Synthesis of Am-1Bi2MmO3m+3 compounds in the Bi4Ti3O12-BiFeO3 system, *Inorg. Mater.* **2002**, *38*, 723-729.

31 Vegard, L. Die Konstitution der Mischkristalle und die Raumfüllung der Atome, *Z. Phys.* **1921**, *5*, 17-26.
32 Chu, M.W.; Caldes, M.T.; Brohan, L.; Ganne, M.; Joubert, M.O.; Piffard, Y. Bulk and Surface Structures of the Aurivillius Phases: Bi4-x La x Ti3O12 (0≤ x≤ 2.00), *Chem. Mater.* **2004**, *16*, 31-42.
33 Koval, V.; Skorvanek, I.; Durisin, J.; Viola, G.; Kovalcikova, A.; Svec jr., P.; Saksl, K.; Yan, H. Terbium-induced phase transitions and weak ferromagnetism in multiferroic bismuth ferite ceramics, *J. Mater. Chem. C* **2017**, *5*, 2669-2685.
34 Newnham, R.E. Cation ordering in Na0.5Bi4.5Ti4O15, *Mater. Res. Bull.* **1967**, *2*, 1041-1044.
35 Khomchenko, V.A.; Kakazei, G.N.; Pogorelov, Y.G.; Araujo, J.P.; Bushinsky, M.V.; Kiselev, D.A., Kholkin, A.I.; Paixao, J.A. Effect of Gd substitution on ferroelectric and magnetic properties of Bi4Ti3O12, *Mat. Lett.* **2010**, *64*, 1066-1068.
36 Mao, X.; Sun, H.; Wang, W.; Lu, Y.; Chen, X. Effects of Co-substitutes on multiferroic properties of Bi5FeTi3O15 ceramics, *Solid State Commun.* **2012**, *152*, 483-487.
37 Kojima, S.; Imaizumi, R.; Hamazaki, S.; Takashige, M. Raman Scattering Study of Bismuth Layer-Structure Ferroelectrics, *Jpn. J. Appl. Phys.* **1994**, *33*, Part 1, 5559-5564.
38 Neaton, J.B.; Ederer, C.; Waghmare, U.V.; Spaldin, N.A.; Rabe, K.M. First-principles study of spontaneous polarization in multiferroic BiFeO3, *Phys. Rev. B* **2005**, *71*, 014113-1-18.
39 Sun, S.; Ling, Y.; Peng, R.; Liu, M.; Mao, X.; Chen, X.; Knize, R. J.; Lu, Y. Synthesis of Ni-substituted Bi7Fe3Ti3O21 ceramics and their superior room temperature multiferroic properties, *RSC Adv.* **2013**, *3*, 18567-18572.
40 Martin, D.H. *Magnetism in Solids*, Iliffe: London, 1967.
41 Jartych, E.; Pikula, T.; Mazurek, M.; Lisinska-Czekaj, A.; Czekaj, D.; Gaska, K.; Przewoznik, J.; Kapusta, C.; Surowiec, Z. Antiferromagnetic spin glass-like behavior in sintered multiferroic Aurivillius Bim+1Ti3Fem−3O3m+3 compounds, *J. Magn. Magn. Mater.* **2013**, *342*, 27-34.
42 Grunes, L.A. Study of the K edges of 3d transition metals in pure and oxide form by x-ray-absorption spectroscopy, *Phys. Rev. B* **1983**, *27*, 2111-2131.
43 Aluri, E.R.; Grosvenor, A.P. An X-ray absorption spectroscopic study of the effect of bond covalency on the electronic structure of Gd2Ti(2-x)Sn(x)O7, *Phys. Chem. Chem. Phys.* **2013**, *15*, 10477-10486.
44 Pikula, T.; Guzdek, P.; Dzik, J.; Lisinska-Czekaj, A.; Jartych, E. X-Ray Diffraction, Mössbauer Spectroscopy, and Magnetoelectric Effect Studies of Multiferroic $Bi_5Ti_3FeO_{15}$ Ceramics, *Acta Phys. Pol. A* **2015**, *127*, 296-299.
45 Koval, V.; Skorvanek, I.; Reece, M.; Mitoseriu. J.; Yan, H. Effect of dysprosium substitution on crystal structure and physical properties of multiferroic BiFeO3 ceramics, *J. European Ceram. Soc.* **2014**, *34*, 641-651.
46 Li, Z.; Ma, J.; Gao, Z.; Viola, G.; Koval, V.; Mahajan, A.; Li, X.; Jia, Ch.; Nan, C.; Yan, H. Room temperature magnetoelectric coupling in intrinsic multiferroic Aurivillius phase textured ceramics, *Dalton Trans.* **2016**, *45*, 14046.

47 Wang, W.; Shen, X.; Wang, W.; Guan, X.; Yao, Y.; Wang, Y.; Yu, R. The Evolution of Microstructure and Magnetic Properties of the Bismuth Layer Compounds with Cobalt Ions Substitution, *Inorg. Chem.* **2017**, *56*, 3207-3213.

48 Giddings, A.; Stennett, M.; Reid, D.; McCabe, E.; Greaves, C.; Hyatt, N. Synthesis, structure and characterization of the n=4 Aurivillius Phase Bi5Ti3CrO15, *J. Solid State Chem.* **2011**, *184*, 252-263.

49 Palizdar, M.; Comyn, T.P.; Ward, M.B.; Brown, A.P.; Harrington, J.P.; Kulkarni, S.; Keeney, L.; Roy, S.; Pemble, M.; Whatmore, R. et al. Crystallographic and magnetic identification of secondary phase in orientated Bi5Fe0.5Co0.5Ti3O15 ceramics, *J. Appl. Phys.* **2012**, *112*, 073919.

50 Li, Z.; Tao, K.; Ma, J.; Gao, Z.; Koval, V.; Jiang, Ch.; Viola, G.; Zhang, H.; Mahajan, A.; Cao, J. et al. Bi3.25La0.75Ti2.5Nb0.25(Fe0.5Co0.5)0.25O12, a single phase room temperature multiferroic, *J. Mat. Chem. C* **2018**, *6*, 2733-2740.

TOC Graphic

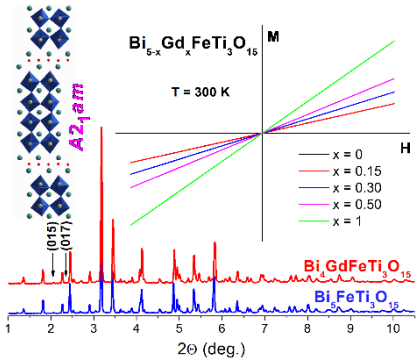
Bi5-xGdxFeTi3O15
M
T = 300 K
H
x = 0
x = 0.15
x = 0.30
x = 0.50
x = 1
A21am
(015)
(017)
Bi4GdFeTi3O15
Bi5FeTi3O15
1
2
3
4
5
6
7
8
9
10
2Θ (deg.)